

CDRL: A Reinforcement Learning Framework Inspired by Cerebellar Circuits and Dendritic Computational Strategies

Sibo Zhang¹ Rui Jing¹ Liangfu Lv¹ Jian Zhang¹ Yunliang Zang¹

Abstract

Reinforcement learning (RL) has achieved notable performance in high-dimensional sequential decision-making tasks, yet remains limited by low sample efficiency, sensitivity to noise, and weak generalization under partial observability. Most existing approaches address these issues primarily through optimization strategies, while the role of architectural priors in shaping representation learning and decision dynamics is less explored. Inspired by structural principles of the cerebellum, we propose a biologically grounded RL architecture that incorporate large expansion, sparse connectivity, sparse activation, and dendritic-level modulation. Experiments on noisy, high-dimensional RL benchmarks show that both the cerebellar architecture and dendritic modulation consistently improve sample efficiency, robustness, and generalization compared to conventional designs. Sensitivity analysis of architectural parameters suggests that cerebellum-inspired structures can offer optimized performance for RL with constrained model parameters. Overall, our work underscores the value of cerebellar structural priors as effective inductive biases for RL.

1. Introduction

Reinforcement learning (RL) has shown remarkable progress in sequential decision-making and control across high-dimensional domains such as Atari, robotics, and complex simulations (Anwar et al., 2022; Graesser et al., 2022). Yet, learning effective policies from raw observations remains challenging due to low sample efficiency, sensitivity to noise, and poor generalization issues exacerbated under partial observability and stochastic perturbations.

¹Academy of Medical Engineering and Translational Medicine, Tianjin University, Tianjin, China. Correspondence to: Yunliang Zang <yunliangzang@tju.edu.cn>.

Existing solutions often rely on advanced training strategies, including auxiliary objectives, data augmentation, regularization, and large-capacity networks (Shakya et al., 2023; Zhu et al., 2023; Zeng et al., 2024). While these can improve optimization and data efficiency, they typically incur high computational cost, require extensive tuning, and pay less attention to how architectural principles shape representation learning and decision-making. This raises a key question: Can network structure itself provide a direct and robust means of addressing the core challenges of high-dimensional RL?

Biological intelligence suggests the answer may be yes: animals and humans learn complex behaviors from sparse, noisy, and partially observable inputs, often with minimal rewards, by leveraging specialized sensory pathways, recurrent dynamics, and adaptive synapses. These neural circuits integrate perception, memory, and action, enabling rapid generalization across tasks without exhaustive retraining.

Recent brain-inspired RL approaches have drawn on models of different brain regions to enhance representation learning, planning, and control. Examples include hippocampus-inspired RL for spatial mapping and episodic memory (Baino et al., 2018; Ritter et al., 2018), prefrontal cortex inspired RL for hierarchical planning and working memory (Wang et al., 2018), and basal ganglia-inspired RL for reward-driven action selection and policy optimization (Joel et al., 2002; Gurney et al., 2015).

The cerebellum plays a key role in sensorimotor control, predictive modeling, and error correction under high-dimensional, noisy, and delayed inputs (Wolpert et al., 1998; Ito, 2006; Zang & De Schutter, 2023). Recent findings show that climbing fibers (CFs) and granule cells (GrCs) convey reward signals, suggesting cerebellar involvement in RL (Wagner et al., 2017; Kostadinov et al., 2019). Its precise timing, adaptive learning rules, and efficient feedforward processing make it a strong model for RL agents requiring rapid adaptation and stable performance in dynamic environments.

The main information path in the cerebellum exhibits a stereotyped feedforward architecture (Fig. 1), mossy fiber (MF) → GrC → purkinje cell (PC) → cerebellar nuclei

(CN)), large expansion ($n_{\text{GrC}} : n_{\text{MF}} \approx 27 : 1$), sparse connectivity (each GrC connects to five MFs), sparse activation (top-k selection) in GrCs, and dendritic-level modulation in PCs that enables state-dependent gating and context-sensitive learning. From a computational perspective, these principles may directly address RL challenges:

- **Large expansion** improves representational separability, aiding downstream value estimation and policy learning.
- **Sparse activation and connectivity** reduce overlap between patterns and suppress irrelevant or noisy features, enhancing robustness in high-dimensional spaces.
- **Dendritic modulation** enables state-dependent gating, supporting conditional computation and adaptability under noise and task variation.

Together, these mechanisms form a powerful set of architectural inductive biases for RL, offering an alternative to conventional deep network designs. In this work, we propose an RL framework inspired by cerebellar circuits and dendritic computational strategies (CDRL). The architecture incorporates large expansion, sparse connectivity, sparse activation, and dendritic-level modulation as network-level priors. We instantiate this architecture within the Double Deep Q-Network (DDQN) framework by replacing the standard Q-network with a cerebellum-inspired value function approximator. We systematically evaluate the architectural features effects on the model’s robustness and generalization in noisy, high-dimensional RL environments, and demonstrate significant improvements over existing architectures.

2. Related Work

Algorithmic advances in RL

A substantial body of research has sought to improve RL performance through algorithmic optimization and training-centric strategies. One widely explored approach focuses on optimization, aiming to refine optimization dynamics and enhance representation quality. Data augmentation has been extensively applied to improve policy robustness, with examples including automatic augmentation selection (Raileanu et al., 2021) and feature-level frame stacking with shifted overlays (Song et al., 2024). Auxiliary objectives have been introduced to enrich state and action representations, such as temporal contrastive learning (Zheng et al., 2023) and dual-agent reward shaping (Ma et al., 2024b). Regularization techniques have also been employed to stabilize training, such as Parseval regularization for weight orthogonality (Chung et al., 2024) and policy-constrained updates in offline settings (Ran et al., 2023).

Another line of research investigates training methodologies that expand model capacity and enable efficient large-scale learning. Scaling model capacity has proven effective in enhancing representation quality and task performance (Bai et al., 2024), while distributed training facilitates efficient large-scale policy optimization (Ma et al., 2024a).

Despite these advances, most approaches remain centered on training dynamics, often introducing computational overhead and heightened sensitivity to hyperparameter selection.

AI Architectures Inspired by Biological Circuits

Biologically inspired neural architectures have profoundly influenced and been widely applied in fields including image classification, motor learning, and robotic arm manipulation.

Visual Processing Pathways: The hierarchical processing observed in the primate ventral visual stream (the “what” pathway), first characterized by Hubel and Wiesel, has directly influenced the design of convolutional neural networks (CNNs) (Hubel & Wiesel, 1959). Subsequent experiments have demonstrated strong similarities between CNN architectures and the ventral visual stream, with state-of-the-art CNN models achieving near-human-level object recognition performance (Yamins & DiCarlo, 2016).

Motor Control and Learning: Inspired by the cerebellum’s role in motor coordination, cerebellar trajectory modules are integrated into robotic manipulation systems. These models enable precise trajectory execution and adaptive motor performance, leading to improved control in dynamic environments (Abadía et al., 2021; Zhang et al., 2022).

Dendritic Neuron Models: Dendrites have the potential of implementing more complicated computations (Zang & De Schutter, 2021). Dendritic branches allow task-dependent gating of relevant features (Veness et al., 2021), while branched neuron designs facilitate rapid adaptation in high-dimensional input spaces (Acharya et al., 2022). More recent studies incorporate nonlinear dendritic gating mechanisms to dynamically integrate information, improving learning efficiency and training stability (Zhang et al., 2024; Chavlis & Poirazi, 2025).

Brain-Inspired RL

Existing brain-inspired studies mainly enhance RL by abstracting neural systems into specific cognitive or functional roles. Representative examples include hippocampus-inspired models for spatial representation and episodic memory (Banino et al., 2018; Ritter et al., 2018), prefrontal cortex-inspired architectures for hierarchical planning and working memory (Wang et al., 2018), and basal ganglia-inspired models for reward-driven action selection and policy optimization (Joel et al., 2002; Gurney et al., 2015). These models highlight the utility of functional abstractions but place relatively less emphasis on architectural priors.

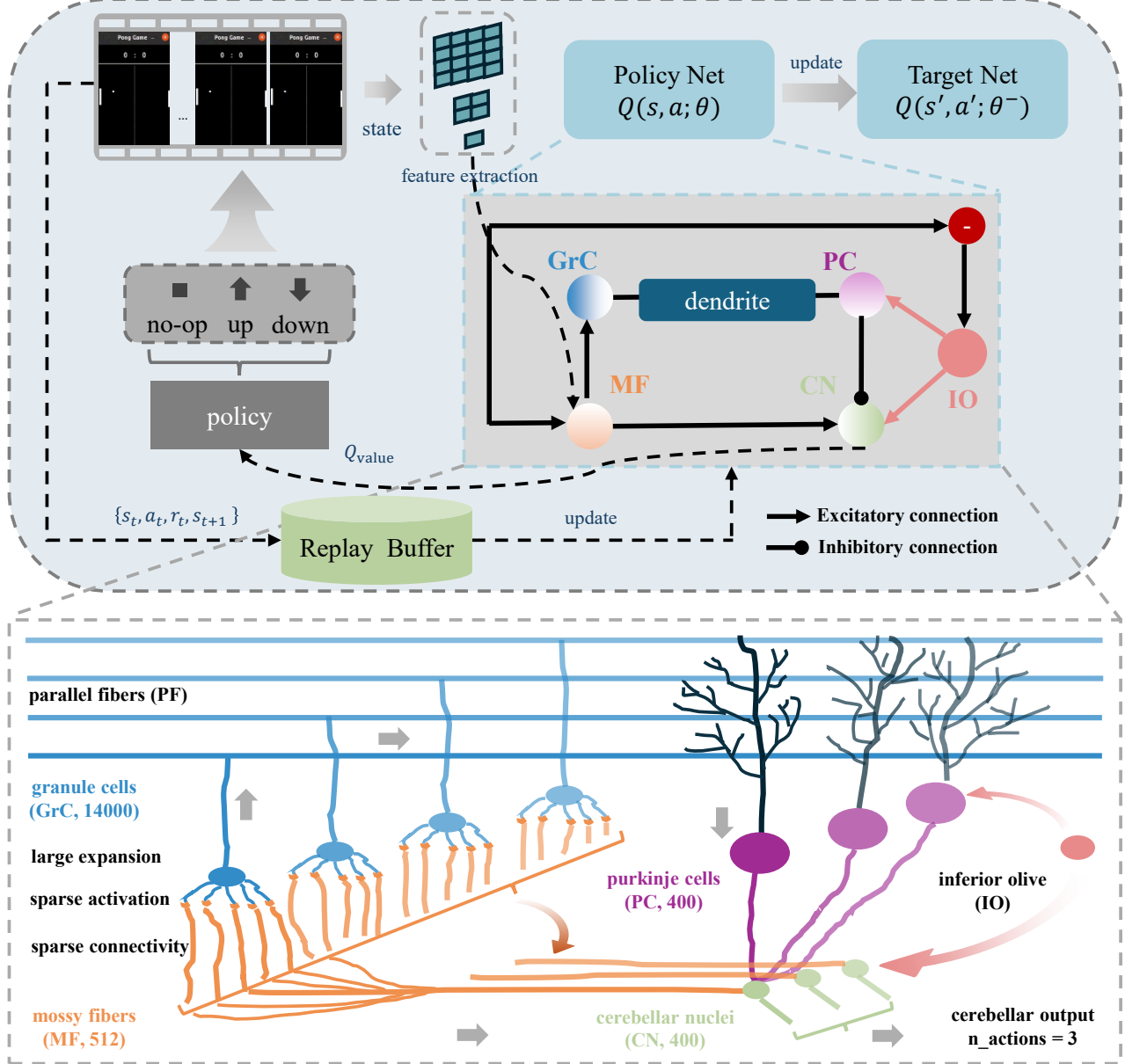


Figure 1. Architecture of the RL framework inspired by cerebellar circuits and dendritic computational strategies.

Previous cerebellum-inspired RL models have attempted to incorporate cerebellar components as auxiliary modules within conventional RL frameworks (Li et al., 2022; Hoang et al., 2025), often relying on simplified cerebellar circuits. Some spiking-based RL models implement biologically grounded learning (Masetty et al., 2021; Kuriyama et al., 2025), but are constrained by the complexity of training and the limited use of cerebellar structural principles, restricting their scalability and performance in complex tasks. Although the cerebellum has been shown to support key RL operations, including state representation, action selection, and evaluative feedback processing (Swain et al., 2011; Kuriyama et al., 2025), existing cerebellum-inspired ap-

proaches rarely leverage its structural organization as architectural priors, thereby limiting their potential for effective representation and decision-making in deep RL.

3. Preliminary and Methodology

3.1. RL Framework

DDQN Algorithm. In our framework, we adopt DDQN (Van Hasselt et al., 2016), which mitigates the over-estimation bias of standard Deep Q-Network (DQN) (Mnih et al., 2015). DQN methods learn a parameterized action-value function $Q(s, a; \theta)$, which estimates the expected cu-

mulative reward (Q_{value}) for taking action a in state s and following a given policy π thereafter. Here, the policy π maps states to actions, which is implicitly induced by the learned Q-function. In practice, this Q-function is approximated by a neural network. DDQN decouples action selection and action evaluation using two separate Q-networks: an online network parameterized by θ and a target network parameterized by θ^- .

The input state is first processed by a three-layer CNN to extract compact spatiotemporal representations. These representations are then fed into the DDQN value estimation module to compute action-value functions. As an off-policy algorithm, DDQN leverages experience replay to learn from past interactions, which further stabilizes training and improves data efficiency (Fig. 1).

Given an input state s , the online network estimates the action-value function $Q(s, a; \theta)$, which represents the expected return of executing action a under the current policy. A greedy policy $\pi(s) = \arg \max_a Q(s, a; \theta)$ is implicitly derived from these estimates and used for action selection during learning and evaluation.

Training is performed by minimizing the mean-squared temporal-difference (TD) error over transitions sampled from the replay buffer \mathcal{D} :

$$\mathcal{L}(\theta) = \mathbb{E}_{(s_t, a_t, r_t, s_{t+1}) \sim \mathcal{D}} \left[(y_t - Q(s_t, a_t; \theta))^2 \right], \quad (1)$$

where the target value y_t is defined as

$$y_t = r_t + \gamma Q(s_{t+1}, \arg \max_{a'} Q(s_{t+1}, a'; \theta^-); \theta^-). \quad (2)$$

The next action is selected by the online network, while its corresponding value is evaluated using the target network, leading to more stable value estimation.

Q-Network. We enhance the standard Q-network in DDQN with a cerebellum-inspired architecture for action-value estimation. This design improves sample efficiency and robustness of value estimation in high-dimensional perceptual control tasks. A dendritic-level modulation mechanism adopted to allow state-dependent regulation, adaptively controlling information flow under observational noise or task variations. All modifications remain fully compatible with the DDQN optimization objective.

3.2. The cerebellar architecture in the framework

In our framework, a high-dimensional perceptual state s_t input is fed into the cerebellar circuit, which outputs a policy distribution $\pi(a_t | s_t)$ through large expansion and state-dependent modulation.

The cerebellar architecture consists of three core components: (i) large expansion implemented via GrC layer, (ii)

sparse MF-GrC connectivity, and (iii) sparse activation in GrCs. Together, these components embed biologically inspired structural inductive biases into the RL framework, the computational procedure of the cerebellar architecture is summarized in Algorithm 1 of the Appendix.

The proposed architecture is designed as a modular and algorithm-agnostic component, and can be trained jointly with standard RL algorithms such as DQN or DDQN to optimize either the action-value function, from which the policy π is implicitly derived.

In our framework, the cerebellar GrCs map the input state from MFs to a high-dimensional feature space. Specifically, given an input vector $x_t \in \mathbb{R}^{d_s}$, where d_s denotes the dimensionality of the input, a sparse random projection $\Phi: \mathbb{R}^{d_s} \rightarrow \mathbb{R}^{d_{GrC}}$ generates sparse activations:

$$\mathbf{h}_{GrC} = \text{ReLU}(\Phi(x_t)) \odot \mathbf{v}, \quad \mathbf{v} \sim \text{Bernoulli}(p), \quad (3)$$

where $d_{GrC} \gg d_s$ and \mathbf{v} is a sparsity mask ensuring most neurons are inactive, enhancing representational capacity and improving generalization. In the cerebellar circuit, each GrC receives inputs from only a small subset of MFs, enforcing structural sparsity to promote pattern separation. Additionally, the GrCs are sparsely activated to facilitate the pattern separation and information capacity. Subsequently, GrCs project to PCs, which target the cerebellar output cells in CN. Because of sparsely activated GrCs, each PC integrates inputs from only a subset of GrC features, forming a local sparse projection:

$$\mathbf{h}_{PC} = \mathbf{W}_{GrC_PC} \mathbf{h}_{GrC}, \quad (4)$$

where the synaptic weight matrix \mathbf{W}_{GrC_PC} is sparse. Together, sparse connectivity and sparse activation reduce information redundancy, suppress noise propagation, and preserve salient features, providing stable and discriminative inputs for downstream decision-making units. In our model, the final output of the CN is computed by the weighted combination of the direct and indirect pathways:

$$\text{CN}_{direct} = f_{MF_CN}(x_t), \quad (5)$$

$$\text{CN}_{indirect} = f_{PC_CN}(\mathbf{h}_{PC}). \quad (6)$$

Subsequently, the cerebellar output is fed into the Q-network for value estimation. The overall training objective follows the standard DDQN formulation defined in Eq. (1). Specifically, the Q-function is parameterized by the proposed cerebellum-inspired network, and optimized by minimizing $\mathcal{L}(\theta)$. θ denotes the set of trainable parameters, including the GrC \rightarrow PC synaptic weights and the fusion weights. The introduction of the cerebellar module does not alter the underlying optimization procedure. Training follows the standard DDQN paradigm with experience replay and ϵ -greedy exploration.

3.3. Dendritic Modulation Mechanism

The computational procedure of the dendritic mechanism, mimicking gating function in PC complex dendrites, is summarized in Algorithm 2 of the Appendix. We implement dendritic mechanisms as a population-driven, non-trainable gain module on the GrC-PC pathway, abstracting sub-branch integration via random hyperplane projections and top-k selection, with slow exponential moving average (EMA) dynamics regulating excitability. This modulates signal amplitude without altering synaptic weights or requiring backpropagation.

Given sparse GrC activations $\mathbf{G}_t \in \mathbb{R}^{B \times D}$ at time t , where B denotes the batch size and D denotes the number of GrC, and $b \in \{1, \dots, B\}$ indexes individual samples within the batch, we compute a population-level representation as:

$$\bar{\mathbf{g}}_t = \frac{1}{B} \sum_{b=1}^B \mathbf{G}_t^{(b)}, \quad \mathbf{G}_t \in \mathbb{R}^{B \times D}. \quad (7)$$

The population activity is ℓ_2 -normalized as:

$$\tilde{\mathbf{g}}_t = \frac{\bar{\mathbf{g}}_t}{\|\bar{\mathbf{g}}_t\|_2}. \quad (8)$$

Each dendritic branch m employs a fixed random hyperplane (Veness et al., 2021) with unit normal $\mathbf{h}_m \in \mathbb{R}^D$ ($\|\mathbf{h}_m\|_2 = 1$), which projects GrC outputs via

$$p_{t,m} = \tilde{\mathbf{g}}_t^\top \mathbf{h}_m, \quad (9)$$

where M denotes the number of dendritic branches. The hyperplanes are fixed and excluded from backpropagation, thereby reducing the training cost.

Only the top-k dendritic branches are activated,

$$\mathcal{S}_t = \text{TopK}(\{p_{t,m}\}_{m=1}^M, K), \quad K = \rho M. \quad (10)$$

The dendritic integration is defined as:

$$\mathbf{d}_t = \sum_{m \in \mathcal{S}_t} \sigma(\beta p_{t,m}) \mathbf{h}_m, \quad (11)$$

yielding the instantaneous dendritic signal:

$$\mathbf{z}_t = \sigma(\mathbf{d}_t). \quad (12)$$

To introduce a slow temporal scale, dendritic signals are accumulated via:

$$\mathbf{e}_t = \tau \mathbf{e}_{t-1} + (1 - \tau) \mathbf{z}_t, \quad \tau \in (0, 1). \quad (13)$$

Finally, the accumulated dendritic state modulates GrC inputs to PCs:

$$\hat{\mathbf{G}}_t = \mathbf{G}_t \odot (\mathbf{1} + \alpha(\mathbf{e}_t - 0.5)). \quad (14)$$

Equations (7)–(14) define a dendritic modulation mechanism that operate on population-level GrC statistics, integrate information across multiple random dendritic branches, and accumulates modulatory signals over a slow temporal scale, while remaining fully decoupled from gradient-based learning.

4. Experiments

4.1. Experimental Setup

Existing implementations lack the flexibility necessary to support interactive environments with configurable physical dynamics. Following common practice in prior works (Adhikari & Ren, 2021; Anwar et al., 2022; Takano et al., 2024; Chen et al., 2025), to address this limitation, we develop a custom Pong environment (Fig. 2) tailored to our experimental requirements which is inspired by Atari Pong. (key parameters in Table 3 of the Appendix).

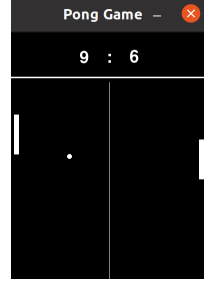


Figure 2. Self-built Pong game environment.

The environment incorporates frame stacking, grayscale preprocessing, and a discrete action space (*up*, *down*, *no-operation*). The left agent follows our trained policy, while the right agent is a built-in controller that tracks and controls the ball's position. Training is conducted using the discrete DDQN with experience replay and ϵ -greedy exploration. Hyperparameters, including learning rate, discount factor (γ), replay buffer size, and batch size, are provided in Table 4 of the Appendix. Rewards are assigned +1 for scoring, -1 for conceding, and 0 otherwise, with each game played to 21 points, yielding a sparse episodic signal. Evaluation metrics include win rate, average reward, robustness under observation noise or action perturbations, and generalization performance across environment variations. Unless stated otherwise, results use five fixed seeds.

To ensure fair comparison, we design a baseline model that shares the same feature-extraction backbone and feedforward network depth as the proposed CDRL model. The key difference is that CDRL incorporates sparse connectivity and sparse activation, reducing the parameter count to ~ 6 M (compared with ~ 13 M for the baseline) and training cost, while achieving higher accuracy and rewards, but the baseline model does not employ any sparsity mechanisms.

Sample Efficiency Evaluation. Sample efficiency is evaluated by measuring learning progress against the number of environment interaction steps rather than episodes. To obtain a stable estimate of performance under the high variance and non-stationary dynamics of RL, we apply EMA to the reward sequence recorded at each training step. EMA assigns larger weights to more recent observations while retaining information from earlier samples.

Formally, let r_t denote the episode reward observed at training step t . The EMA-smoothed reward \hat{r}_t is computed recursively as

$$\hat{r}_t = \alpha r_t + (1 - \alpha)\hat{r}_{t-1}, \quad (15)$$

where $\alpha \in (0, 1]$ controls the decay rate of past observations. A larger α emphasizes recent rewards, while a smaller value yields stronger smoothing over longer horizons.

Robustness Evaluation. To evaluate the robustness of our framework, we introduce controlled perturbations during evaluation while keeping the training environment unchanged. Specifically, Gaussian observation noise (Zhang et al., 2020) is added to the agent’s perceptual input:

$$\tilde{s}_t = s_t + \epsilon_t, \quad \epsilon_t \sim \mathcal{N}(0, \sigma^2), \quad (16)$$

where s_t denotes the original observation and \tilde{s}_t is the corrupted observation. In addition, random action perturbations (Tessler et al., 2019; Lyle et al., 2022) are applied to simulate execution noise under realistic conditions, where the selected action is stochastically replaced with a random action with a fixed probability.

Notably, both observation noise and action perturbations are applied only to the evaluated agent. The opponent follows a deterministic position-tracking policy and is not affected by these perturbations. Under this asymmetric configuration, we focus on comparing the relative robustness gains of the cerebellum-inspired model and the dendritic-augmented model with respect to the baseline. This design ensures that observed robustness improvements arise from the intrinsic structural advantages of the proposed architectures rather than from reduced task difficulty.

We further evaluate the models under a sticky action noise setting, with a stickiness parameter of 0.25, which introduces a probability that the agent’s previous action is repeated in the current step. Sticky noise increases action execution uncertainty, simulating the challenge of precise control and providing a rigorous test of policy robustness.

Generalization Evaluation. As shown in Table 1, generalization performance is assessed by modifying predefined environment parameters at test time, including the ball velocity, decomposed into horizontal and vertical components (Ball Spd. (H) and Ball Spd. (V)), as well as the paddle

length (Paddle Len.) and paddle movement speed (Paddle Spd.). These variations induce systematic changes in environment dynamics while preserving the task objective. The agent’s performance on unseen configurations evaluates its generalization beyond the training distribution.

Table 1. Environment parameters used for evaluating model generalization.

Param.	Ball Spd. (H)	Ball Spd. (V)	Paddle Len.	Paddle Spd.
Train	12	8	80	5
Test 1	15	10	80	5
Test 2	18	12	80	5
Test 3	12	8	60	5
Test 4	12	8	20	5
Test 5	12	8	80	2
Test 6	12	8	80	3
Test 7	12	8	80	4

4.2. CDRL Model Evaluation

We first assess sample efficiency to measure the CDRL’s fundamental learning performance, then examine robustness under stochastic perturbations to evaluate stability, and finally evaluate generalization to novel conditions to assess the model’s ability to maintain performance in unseen scenarios.

4.2.1. SAMPLE EFFICIENCY TESTING

In Figure 3, we compare the reward dynamics of CDRL, CDRL-dendrite (with dendritic components removed), and the baseline model during training. CDRL achieves a higher steady-state reward more quickly than the other two models, demonstrating superior sample efficiency. In contrast, the reward performance of CDRL-dendrite saturates faster and at a higher level compared to the baseline model. These results indicate that both cerebellum-inspired and dendritic mechanisms contribute to more effective policy acquisition under limited interaction data.

4.2.2. ROBUSTNESS TESTING

For robustness testing, models are trained in the customized Pong environment and evaluated under stochastic perturbations applied to both observations and actions. Figure 4 illustrates the difference in win rate between the CDRL model and the baseline model. Positive values indicate cases where CDRL outperforms the baseline. Across a wide range of observation noise levels (0.00–10.00) and action perturbation probabilities (0.00–0.30), CDRL consistently demonstrate superior robustness compared to baseline. The win rates of CDRL and baseline under different combinations of noise parameters are reported in Table 5 of the Appendix. In addition, the CDRL-dendrite model also ex-

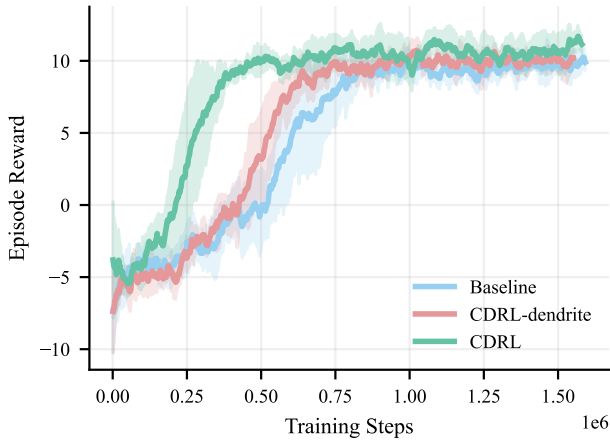


Figure 3. Sample efficiency of different models during training, measured by performance versus number of training steps.

hibits superior robustness under most test conditions relative to baseline, suggesting that both the cerebellar architecture and dendritic mechanisms contribute to the robustness improvements. Detailed results are provided in Table 6 of the Appendix.

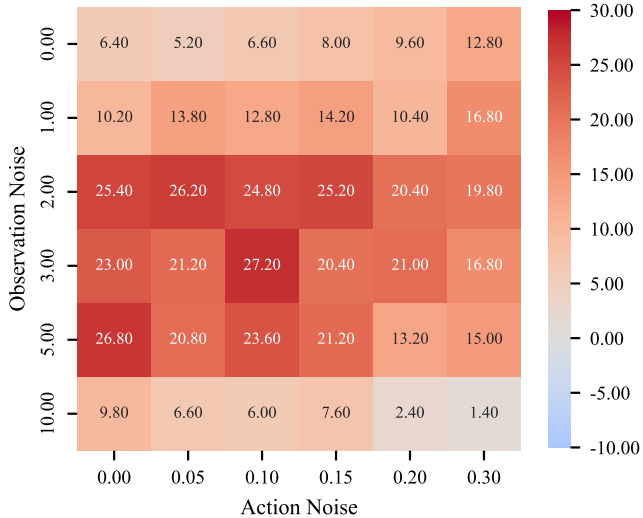


Figure 4. Heat map of the difference in robustness between the CDRL model and the baseline model.

Table 2 summarizes the performance of baseline, CDRL-dendrite, and CDRL models under sticky action noise setting. Across multiple trials, the CDRL model consistently achieves the highest win rate and average reward, outperforming both the baseline and CDRL-dendrite models. These results highlight the effectiveness of cerebellum-inspired architecture and the dendritic-level modulation

mechanism in enhancing policy robustness under noises.

Table 2. Performance under sticky action noise ($p = 0.25$).

Model	Baseline	CDRL-dendrite	CDRL
win rate (%)	91.20 ± 3.54	97.20 ± 1.47	97.60 ± 1.85
reward	8.38 ± 0.85	9.71 ± 0.50	10.07 ± 1.97

4.2.3. GENERALIZATION TESTING

As shown in Figure 5, across three configuration variations: ball speed (tests 1–2), paddle length (tests 3–4), and paddle speed (tests 5–7), CDRL consistently achieves the highest win rate in the test stage, followed by CDRL-dendrite, with the baseline model performing the lowest. These results indicate that both the cerebellar architecture and dendritic modulation contribute to the superior generalization observed in the CDRL model.

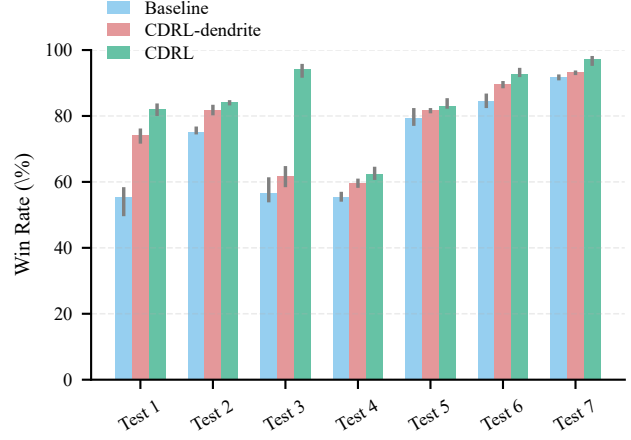


Figure 5. Generalization performance of different models under unseen environment configurations.

4.3. Sensitivity Analysis of the Cerebellar Architectural Features

The architecture of CDRL possesses several critical features, including the GrC layer expansion ratio, sparse connection, and sparse activation. In biological circuits, these features may be constrained by developmental cost and functional requirements. However, the parameter settings underlying these features may not be optimal for RL tasks, particularly in high-dimensional perceptual domains. To quantify the impact of each feature on model performance and guide the design of cerebellum-inspired architectures for RL, we conduct a series of sensitivity tests by selectively removing or modifying one key feature at a time.

Expansion Ratio. In Figure 6, all tested model variants achieve a higher win rate than the baseline. The model with

16,384 GrCs demonstrates stronger robustness than CDRL in the medium noise range but shows no advantage in the low or high noise ranges. Given the larger computational load (parameters) associated with the more expanded architecture, the cerebellar design may offer a reasonable trade-off between performance and computational cost. By enhancing feature representation and pattern separation (Zou et al., 2025a), a modestly large expansion can improve RL performance while maintaining acceptable computational overhead.

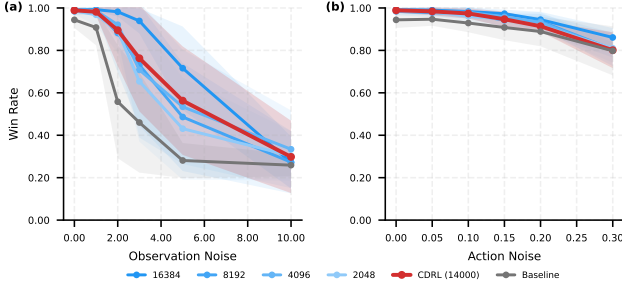


Figure 6. Sensitivity results of the expansion ratio. (a) Observation noise. (b) Action noise.

Sparse mechanisms. In the cerebellar architecture, each GrC receives inputs from only a small subset of MFs. Such sparse projections reduce overlap between different contexts and attenuate observation noise, limiting its propagation and preventing small perturbations from influencing all GrCs. The benefit of sparse connection is minimal in the low-noise range (Fig. 7a). However, the model with sparse connection demonstrates superior robustness when noise levels are high. Among the evaluated variants, the CDRL model consistently outperforms the baseline (fully connected) across all observation noise levels. As expected, the degree of connection sparsity does not significantly affect model performance under action-noise conditions (Fig. 7b). Overall, these results suggest that sparse connections should be prioritized due to their lower computational cost (parameters) and superior performance.

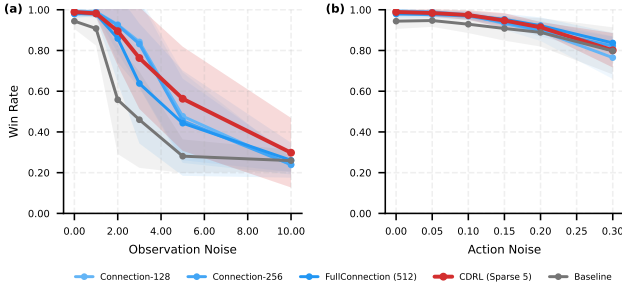


Figure 7. Sensitivity results of the sparse connectivity. (a) Observation noise. (b) Action noise.

Cerebellar GrCs are sparsely activated, with only a small fraction active at any given time. This property has been shown to be critical in tasks such as continual learning and multitask learning (Zou et al., 2025b;c). In our sensitivity analysis, the CDRL model consistently outperforms the baseline model (without top-k). It also lies within a high-performance range compared to other model variants with denser GrC activation. However, the GrC activation level does not significantly affect model performance under action-noise conditions. In summary, these results suggest that sparse activation in GrCs should be prioritized due to its overall performance.

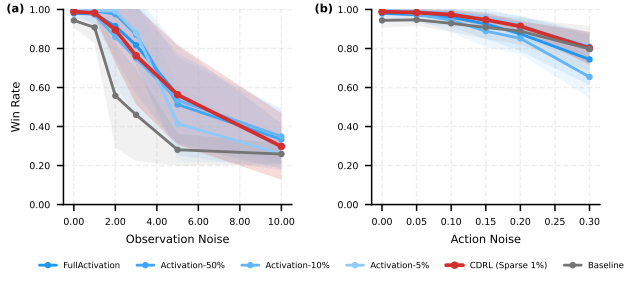


Figure 8. Sensitivity results of the sparse activation. (a) Observation noise. (b) Action noise.

5. Conclusion and Future Work

In this work, we developed a cerebellum-based RL model for a high-dimensional perceptual version of the Pong game with discrete actions. Our results highlight the critical role of the cerebellar architecture and dendritic computation mechanisms in improving win rate, cumulative reward, robustness, and generalization. Sensitivity analysis suggests that the cerebellum provides an optimized structure for RL, although increasing the expansion ratio can enhance performance at the cost of higher computational demand.

Our experiments were limited to the Pong environment with a discrete DDQN framework, constraining task complexity. Continuous-action tasks and high-degree-of-freedom environments remain unexplored. Future work could investigate the architecture’s transferability, its applicability to continuous control tasks such as robotic manipulation, and its performance in multi-task learning and knowledge transfer scenarios. Incorporating online plasticity mechanisms or training under high-noise and delayed-feedback conditions could further assess and improve robustness and generalization.

Overall, this work demonstrates the potential of cerebellar circuits and dendritic strategies as computational inductive biases in RL and offers promising directions for broader application across more complex tasks.

Impact Statement

By integrating cerebellum-inspired structural priors into reinforcement learning architectures, we achieve significant improvements in sample efficiency, robustness, and generalization on noisy, high-dimensional tasks with minimal computational overhead. This work highlights the potential of biologically grounded architectural design as an effective inductive bias for advancing deep RL.

References

Abadía, I., Náveros, F., Ros, E., Carrillo, R. R., and Luque, N. R. A cerebellar-based solution to the nondeterministic time delay problem in robotic control. *Science Robotics*, 6(58):eabf2756, 2021.

Acharya, J., Basu, A., Legenstein, R., Limbacher, T., Poirazi, P., and Wu, X. Dendritic computing: branching deeper into machine learning. *Neuroscience*, 489: 275–289, 2022.

Adhikari, A. and Ren, Y. Rl-pong: Playing pong from pixels, 2021.

Anwar, H., Caby, S., Dura-Bernal, S., D’Onofrio, D., Hasegan, D., Deible, M., Grunblatt, S., Chadderton, G. L., Kerr, C. C., Lakatos, P., et al. Training a spiking neuronal network model of visual-motor cortex to play a virtual racket-ball game using reinforcement learning. *Plos one*, 17(5):e0265808, 2022.

Bai, H., Xu, M., Ye, K., Buyya, R., and Xu, C. Drpc: Distributed reinforcement learning approach for scalable resource provisioning in container-based clusters. *IEEE Transactions on Services Computing*, 2024.

Banino, A., Barry, C., Uria, B., Blundell, C., Lillicrap, T., Mirowski, P., Pritzel, A., Chadwick, M. J., Degris, T., Modayil, J., et al. Vector-based navigation using grid-like representations in artificial agents. *Nature*, 557(7705): 429–433, 2018.

Chavlis, S. and Poirazi, P. Dendrites endow artificial neural networks with accurate, robust and parameter-efficient learning. *Nature communications*, 16(1):943, 2025.

Chen, R., Kunde, G. J., Tao, L., and Sornborger, A. T. Foveal vision reduces neural resources in agent-based game learning. *Frontiers in Neuroscience*, 19:1547264, 2025.

Chung, W., Cherif, L., Meger, D., and Precup, D. Parseval regularization for continual reinforcement learning. *Advances in Neural Information Processing Systems*, 37: 127937–127967, 2024.

Graesser, L., Evcı, U., Elsen, E., and Castro, P. S. The state of sparse training in deep reinforcement learning. In *International Conference on Machine Learning*, pp. 7766–7792. PMLR, 2022.

Gurney, K. N., Humphries, M. D., and Redgrave, P. A new framework for cortico-striatal plasticity: behavioural theory meets in vitro data at the reinforcement-action interface. *PLoS biology*, 13(1):e1002034, 2015.

Hoang, H., Tsutsumi, S., Matsuzaki, M., Kano, M., Toyama, K., Kitamura, K., and Kawato, M. Predictive reward-prediction errors of climbing fiber inputs integrate modular reinforcement learning with supervised learning. *PLOS Computational Biology*, 21(3):e1012899, 2025.

Hubel, D. H. and Wiesel, T. N. Receptive fields of single neurones in the cat’s striate cortex. *The Journal of physiology*, 148(3):574, 1959.

Ito, M. Cerebellar circuitry as a neuronal machine. *Progress in neurobiology*, 78(3-5):272–303, 2006.

Joel, D., Niv, Y., and Ruppin, E. Actor-critic models of the basal ganglia: New anatomical and computational perspectives. *Neural networks*, 15(4-6):535–547, 2002.

Kostadinov, D., Beau, M., Blanco-Pozo, M., and Häusser, M. Predictive and reactive reward signals conveyed by climbing fiber inputs to cerebellar purkinje cells. *Nature neuroscience*, 22(6):950–962, 2019.

Kuriyama, R., Yoshimura, H., and Yamazaki, T. A theory of cerebellar learning as spike-based reinforcement learning in continuous time and space. *PNAS nexus*, 4(10): pgaf302, 2025.

Li, H., Liu, R., Wang, Y., Liu, Y., Chen, Y., Wang, J., and Gu, J. A td-learning based bionic cerebellar model controller for humanoid robots. *Procedia Computer Science*, 209: 132–139, 2022.

Lyle, C., Rowland, M., Dabney, W., Kwiatkowska, M., and Gal, Y. Learning dynamics and generalization in deep reinforcement learning. In *International conference on machine learning*, pp. 14560–14581. PMLR, 2022.

Ma, C., Li, A., Du, Y., Dong, H., and Yang, Y. Efficient and scalable reinforcement learning for large-scale network control. *Nature Machine Intelligence*, 6(9):1006–1020, 2024a.

Ma, H., Sima, K., Vo, T. V., Fu, D., and Leong, T.-Y. Reward shaping for reinforcement learning with an assistant reward agent. In *Forty-first international conference on machine learning*, 2024b.

Masetty, B., Mirsky, R., Deshpande, A., Mauk, M., and Stone, P. Is the cerebellum a model-based reinforcement learning agent? In *20th International Conference on Autonomous Agents and Multiagent Systems*, 2021.

Mnih, V., Kavukcuoglu, K., Silver, D., Rusu, A. A., Veness, J., Bellemare, M. G., Graves, A., Riedmiller, M., Fidjeland, A. K., Ostrovski, G., et al. Human-level control through deep reinforcement learning. *nature*, 518(7540):529–533, 2015.

Raileanu, R., Goldstein, M., Yarats, D., Kostrikov, I., and Fergus, R. Automatic data augmentation for generalization in reinforcement learning. *Advances in Neural Information Processing Systems*, 34:5402–5415, 2021.

Ran, Y., Li, Y.-C., Zhang, F., Zhang, Z., and Yu, Y. Policy regularization with dataset constraint for offline reinforcement learning. In *International conference on machine learning*, pp. 28701–28717. PMLR, 2023.

Ritter, S., Wang, J., Kurth-Nelson, Z., Jayakumar, S., Blundell, C., Pascanu, R., and Botvinick, M. Been there, done that: Meta-learning with episodic recall. In *International conference on machine learning*, pp. 4354–4363. PMLR, 2018.

Shakya, A. K., Pillai, G., and Chakrabarty, S. Reinforcement learning algorithms: A brief survey. *Expert Systems with Applications*, 231:120495, 2023.

Song, W., Choi, H., Sohn, K., and Min, D. A simple framework for generalization in visual rl under dynamic scene perturbations. *Advances in Neural Information Processing Systems*, 37:121790–121826, 2024.

Swain, R. A., Kerr, A. L., and Thompson, R. F. The cerebellum: a neural system for the study of reinforcement learning. *Frontiers in behavioral neuroscience*, 5:8, 2011.

Takano, T., Kera, H., and Kawamoto, K. Robustness verification of decision transformer with varying noise-augmented data ratios in atari games. In *International Symposium on Computational Intelligence and Industrial Applications*, pp. 262–273. Springer, 2024.

Tessler, C., Efroni, Y., and Mannor, S. Action robust reinforcement learning and applications in continuous control. In *International Conference on Machine Learning*, pp. 6215–6224. PMLR, 2019.

Van Hasselt, H., Guez, A., and Silver, D. Deep reinforcement learning with double q-learning. In *Proceedings of the AAAI conference on artificial intelligence*, volume 30, 2016.

Veness, J., Lattimore, T., Budden, D., Bhoopchand, A., Mattern, C., Grabska-Barwinska, A., Sezener, E., Wang, J., Toth, P., Schmitt, S., et al. Gated linear networks. In *Proceedings of the AAAI conference on artificial intelligence*, volume 35, pp. 10015–10023, 2021.

Wagner, M. J., Kim, T. H., Savall, J., Schnitzer, M. J., and Luo, L. Cerebellar granule cells encode the expectation of reward. *Nature*, 544(7648):96–100, 2017.

Wang, J. X., Kurth-Nelson, Z., Kumaran, D., Tirumala, D., Soyer, H., Leibo, J. Z., Hassabis, D., and Botvinick, M. Prefrontal cortex as a meta-reinforcement learning system. *Nature neuroscience*, 21(6):860–868, 2018.

Wolpert, D. M., Miall, R. C., and Kawato, M. Internal models in the cerebellum. *Trends in cognitive sciences*, 2(9):338–347, 1998.

Yamins, D. L. and DiCarlo, J. J. Using goal-driven deep learning models to understand sensory cortex. *Nature neuroscience*, 19(3):356–365, 2016.

Zang, Y. and De Schutter, E. The cellular electrophysiological properties underlying multiplexed coding in purkinje cells. *Journal of Neuroscience*, 41(9):1850–1863, 2021.

Zang, Y. and De Schutter, E. Recent data on the cerebellum require new models and theories. *Current Opinion in Neurobiology*, 82:102765, 2023.

Zeng, Y., Cai, R., Sun, F., Huang, L., and Hao, Z. A survey on causal reinforcement learning. *IEEE Transactions on Neural Networks and Learning Systems*, 2024.

Zhang, H., Chen, H., Xiao, C., Li, B., Liu, M., Boning, D., and Hsieh, C.-J. Robust deep reinforcement learning against adversarial perturbations on state observations. *Advances in neural information processing systems*, 33:21024–21037, 2020.

Zhang, J., Chen, J., Wu, W., and Qiao, H. A cerebellum-inspired prediction and correction model for motion control of a musculoskeletal robot. *IEEE Transactions on Cognitive and Developmental Systems*, 15(3):1209–1223, 2022.

Zhang, Y., Cai, P., Sun, Y., Zhang, Z., Lei, Z., and Gao, S. A lightweight multidendritic pyramidal neuron model with neural plasticity on image recognition. *IEEE Transactions on Artificial Intelligence*, 5(9):4415–4427, 2024.

Zheng, R., Wang, X., Sun, Y., Ma, S., Zhao, J., Xu, H., Daumé III, H., and Huang, F. Temporal latent action-driven contrastive loss for visual reinforcement learning. *Advances in Neural Information Processing Systems*, 36:48203–48225, 2023.

Zhu, Z., Lin, K., Jain, A. K., and Zhou, J. Transfer learning in deep reinforcement learning: A survey. *IEEE Transactions on Pattern Analysis and Machine Intelligence*, 45(11):13344–13362, 2023.

Zou, H., Zang, Y., and Ji, X. Structural features of the fly olfactory circuit mitigate the stability-plasticity dilemma in continual learning. *arXiv preprint arXiv:2502.01427*, 2025a.

Zou, H., Zang, Y., Xu, W., and Ji, X. Fly-cl: A fly-inspired framework for enhancing efficient decorrelation and reduced training time in pre-trained model-based continual representation learning. *arXiv preprint arXiv:2510.16877*, 2025b.

Zou, H., Zang, Y., Xu, W., Zhu, Y., and Ji, X. Flylora: Boosting task decoupling and parameter efficiency via implicit rank-wise mixture-of-experts. *arXiv preprint arXiv:2510.08396*, 2025c.

A. Algorithm

A.1. Cerebellar Architecture

Algorithm 1 presents the computational procedure of the cerebellum-inspired feedforward network, highlighting the large expansion in the GrC layer, sparse MF–GrC connectivity, and GrC sparse activation.

Algorithm 1 Cerebellar Architecture

Input: state x , network parameters θ
Output: action logits y
 $feature \leftarrow \text{Feature Extractor}(x)$
 $mf \leftarrow \text{MF}(feature)$
 $gc \leftarrow \text{GrC}(mf; \mathcal{M}_{mf \rightarrow gc})$
 $gc_{\text{sparse}} \leftarrow \text{Sparse Activate}(gc)$
 $pc_out \leftarrow \alpha_{pc} \cdot \text{Purkinje}(gc_{\text{sparse}})$
 $cn_excite \leftarrow \text{MF_to_CN}(feature)$
 $cn \leftarrow \text{clamp}(cn_excite + pc_out, \min = 0)$
 $y \leftarrow \text{CN output layer}(cn)$
return y

A.2. Dendritic Modulation Mechanism

Algorithm 2 presents the computational flow of the dendritic modulation mechanism.

Algorithm 2 Dendritic Modulation Mechanism

Input: GrC activations h_{gc} , dendritic parameters Θ_d
Output: modulated activations x_{mod} , global_gain
 $agg \leftarrow \text{Aggregate}(h_{gc})$
 $b \leftarrow \text{Select Branches}(agg; \Theta_d)$
 $g_{\text{inst}} \leftarrow \text{Dendritic Gate}(b)$
 $g \leftarrow \text{Temporal Integrate}(g_{\text{inst}})$
 $x_{\text{mod}} \leftarrow x \odot \text{Gain}(g)$
 $global_gain \leftarrow \text{Global Gain}(g)$
return $x_{\text{mod}}, global_gain$

B. Parameters

B.1. Pong game environment parameters

Table 3 lists the key parameters of the Pong game environment, such as the ball speed, paddle length, frames per second (FPS), and the frame stack size used during training.

Table 3. Custom Pong environment parameters.

Parameter	Value	Parameter	Value	Parameter	Value
Ball X speed	12	Paddle width	10	Ball Y speed	8
Paddle height	80	Paddle speed	5	FPS	1920
Max score	21	Action noise	0.0	Stack size	4

B.2. Training parameters

Table 4 lists the key training parameters used in our experiments, including the model configuration, learning and exploration settings, and other training hyperparameters. All experiments reported in this paper were performed on NVIDIA RTX 4090 GPUs.

Table 4. Training parameters.

Parameter	Value	Parameter	Value
Model type	Baseline / CDRL	GPU ID	0 / 1
Input channels	4	Batch size	64
Num episodes	1500	Gamma	0.99
Epsilon start	1.0	Epsilon end	0.01
Epsilon decay	200000	Learning rate	5e-07
Memory size	100000	Dendritic gate	Enabled / Disabled
Target update freq	1000	Save every	500

C. Robustness Testing

Table 5 presents the robustness evaluation of the baseline and CDRL models, with bold entries indicating the win rate performance of the CDRL model. Observation noise (Obs) refers to Gaussian noise added to the agent's perceptual input, with a magnitude ranging from 0.00 to 10.00. While action noise (Act) denotes the probability of stochastic perturbations applied to the agent's actions, ranging from 0.00 to 0.30. The results show that the CDRL model outperforms the baseline model.

Table 5. Win rate comparison of the CDRL model and the baseline model under different observation and action noise.

Obs / Act	0.00	0.05	0.10	0.15	0.20	0.30
0.00	0.92±0.04 0.99±0.01	0.93±0.04 0.98±0.01	0.90±0.04 0.97±0.02	0.87±0.07 0.95±0.03	0.84±0.06 0.93±0.02	0.73±0.13 0.86±0.04
1.00	0.88±0.11 0.98±0.01	0.83±0.16 0.96±0.01	0.84±0.11 0.96±0.03	0.80±0.14 0.94±0.03	0.79±0.15 0.89±0.06	0.62±0.09 0.79±0.08
2.00	0.58±0.31 0.84±0.22	0.54±0.29 0.81±0.25	0.54±0.31 0.79±0.25	0.51±0.29 0.76±0.25	0.52±0.23 0.72±0.22	0.42±0.21 0.62±0.20
3.00	0.50±0.29 0.73±0.26	0.48±0.30 0.70±0.27	0.45±0.23 0.72±0.24	0.46±0.25 0.66±0.25	0.40±0.21 0.61±0.23	0.40±0.18 0.57±0.21
5.00	0.30±0.09 0.56±0.25	0.33±0.05 0.54±0.23	0.30±0.07 0.54±0.22	0.28±0.07 0.49±0.21	0.32±0.04 0.46±0.23	0.29±0.07 0.44±0.20
10.00	0.27±0.07 0.37±0.22	0.31±0.06 0.38±0.18	0.29±0.06 0.35±0.19	0.26±0.06 0.34±0.17	0.28±0.04 0.31±0.15	0.27±0.01 0.28±0.14

Table 6 presents the robustness evaluation of the baseline and CDRL-dendrite models, with bold rows indicating the win

rate of the CDRL-dendrite model under different combinations of observation and action noise. The results show that the CDRL-dendrite model consistently achieves higher win rate than the baseline across most test conditions.

Table 6. Win rate comparison of the CDRL-dendrite model and the baseline model under different observation and action noise.

Obs / Act	0.00	0.05	0.10	0.15	0.20	0.30
0.00	0.92±0.04 1±0.01	0.93±0.04 0.97±0.01	0.90±0.04 0.96±0.03	0.87±0.07 0.97±0.01	0.84±0.06 0.95±0.03	0.73±0.13 0.92±0.05
1.00	0.88±0.11 0.90±0.10	0.83±0.16 0.92±0.08	0.84±0.11 0.90±0.09	0.80±0.14 0.91±0.08	0.79±0.15 0.88±0.09	0.62±0.09 0.85±0.09
2.00	0.58±0.31 0.62±0.24	0.54±0.29 0.64±0.23	0.54±0.31 0.63±0.27	0.51±0.29 0.62±0.27	0.52±0.23 0.59±0.24	0.42±0.21 0.60±0.21
3.00	0.50±0.29 0.48±0.23	0.48±0.30 0.51±0.26	0.45±0.23 0.46±0.26	0.46±0.25 0.51±0.21	0.40±0.21 0.46±0.24	0.40±0.18 0.49±0.20
5.00	0.30±0.09 0.34±0.24	0.33±0.05 0.31±0.23	0.30±0.07 0.33±0.24	0.28±0.07 0.30±0.18	0.32±0.04 0.31±0.18	0.29±0.07 0.32±0.15
10.00	0.27±0.07 0.29±0.05	0.31±0.06 0.28±0.04	0.29±0.06 0.31±0.07	0.26±0.06 0.31±0.08	0.28±0.04 0.28±0.06	0.27±0.01 0.27±0.06

D. Code Availability

To facilitate reproducibility, the code and experimental setups for the CDRL framework will be made publicly available following publication.